Feel the Heat: Nonlinear Electrothermal Feedback in Organic LEDs

Axel Fischer, Thomas Koprucki, Klaus Gärtner, Max L. Tietze, Jacqueline Brückner, Björn Lüssem, Karl Leo, Annegret Glitzky, and Reinhard Scholz*

For lighting applications, organic light-emitting diodes (OLED) need much higher brightness than for displays, leading to self-heating. Due to the temperature-activated transport in organic semiconductors, this can result in brightness inhomogeneities and catastrophic failure. Here, it is shown that due to the strong electrothermal feedback of OLEDs, the common spatial current and voltage distribution is completely changed, requiring advanced device modeling and operation concepts. This study clearly demonstrates the effect of S-shaped negative differential resistance in OLEDs induced by self-heating. As a consequence, for increasing voltage, regions with declining voltages are propagating through the device, and even more interestingly, a part of these regions show even decreasing currents, leading to strong local variation in luminance. The expected breakthrough of OLED lighting technology will require an improved price performance ratio, and the realization of modules with very high brightness but untainted appearance is considered to be an essential step into this direction. Thus, a deeper understanding of the control of electrothermal feedback will help to make OLEDs in lighting more competitive.

1. Introduction

Organic light-emitting diodes (OLED) are commercially successful and are used in high-end displays in mobile phones and TV applications. The advantages of this technology are low material costs, low processing temperatures, high luminous efficacy,[1] and large area production. OLEDs are fabricated by depositing different functional layers in between two planar electrodes, typically called sandwich-type geometry.[2] The function of the layers includes charge injection, charge transport, exciton recombination, or charge blocking barriers. White OLEDs have the potential for high quality lighting, but the respective products have not found their way into mass market yet.[3] In 2009, Reineke et al. realized a white OLED with 90 lm W^{-1} at a brightness of 1000 cd m^{-2}.[4] OLED manufacturers have announced white light OLED tiles with a luminous efficacy of 80 lm W^{-1} and a homogeneous brightness of ≈ 3000 cd m^{-2}.[5] Despite this progress, for several applications like general lighting, the costs per module are still too high. For that reason, if OLED tiles would reach 5000 to 10 000 cd m^{-2}, resulting in an overall better price to performance ratio, this would help to access a larger market.

OLEDs can indeed reach this luminance, but on large areas two main aspects prevent the realization. Firstly, the more transparent electrode has a rather high sheet resistance. This will lead to a voltage drop along this electrode, darkening the center of the panel with respect to the edges. This can be overcome by supporting the transparent electrode with a highly conductive mesh grid.[6–8] Secondly, Joule self-heating will appear at much lower brightness due to the large dimensions. Regions which heat up most strongly have an increased conductivity of the OLED layers so that these areas could become somewhat brighter. In the beginning, both effects can counteract each other, since they have an opposite influence onto the brightness in the center of the lighting panel. However, with rising temperature, OLED panels tend to show extreme brightness inhomogeneities. An improved heat conduction into the environment can help,[9–13] but this would mean to relinquish well established procedures like fabrication on glass substrate or plastic foils.

The best solution would be to increase the luminous efficacy of the OLEDs as argued by Sasabe and Kido,[14] leading to higher brightness, lower self-heating, and of course a more economic conversion of electrical power into light. However, state-of-the-art OLEDs are already highly optimized, raising the question whether a further performance increase by a factor of 2–3 can be realized. Another approach is to accept the self-heating with the benefit that higher currents are driven, allowing to reach higher light output. Several publications show simulations of self-heating in OLEDs, and some of them consider electrothermal modeling, demonstrating that self-heating

A. Fischer, M. L. Tietze, Dr. B. Lüssem, Prof. K. Leo, Dr. R. Scholz
Institut für Angewandte Photophysik (IAPP)
Technische Universität Dresden, George-Bähr-Straße 1
01069 Dresden, Germany
E-mail: axel.fischer@iapp.de
Dr. T. Koprucki, Dr. K. Gärtner, Dr. A. Glitzky
Weierstraß-Institut für Angewandte Analysis und Stochastik (WIAS)
Mohrenstraße 39
10117 Berlin, Germany
Dr. J. Brückner, Prof. K. Leo
Fraunhofer COMEDD, Maria-Reiche-Str. 2
01109 Dresden, Germany

DOI: 10.1002/adfm.201303066

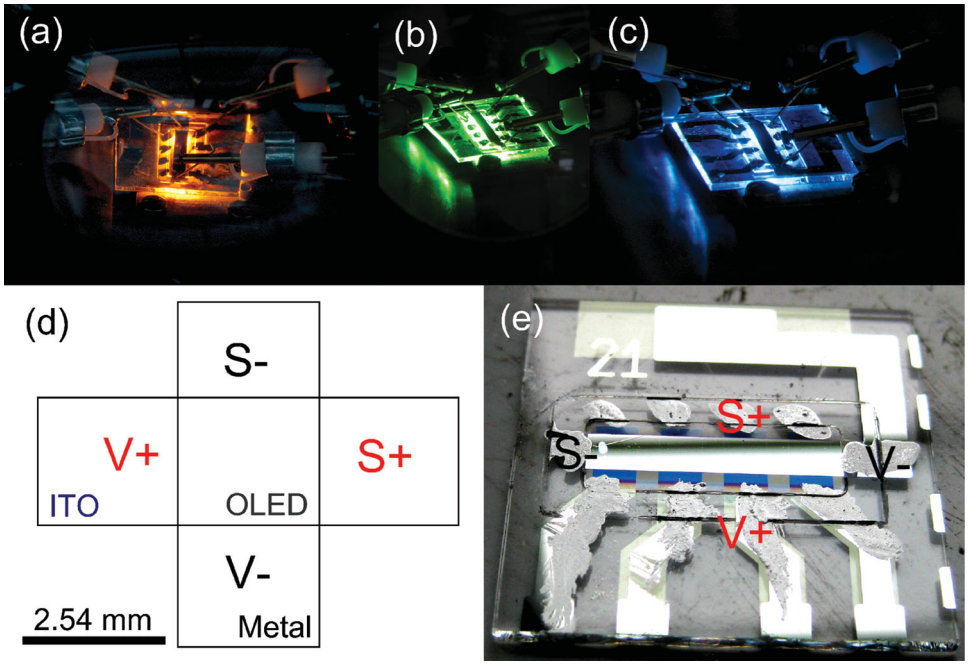

Figure 1. a–c) Pictures of a red, green, and blue OLED during 4-wire crossbar measurement. d) Setup of the 4-wire crossbar measurement. The external voltage *V* is applied between *V*+ and *V*-. The contacts *S*+ and *S*- are used to detect the voltage *S* at the backside of the device. e) Decapsulated sample after measurement. Liquid silver covers the contacts to minimize residual contact resistances.

causes brightness inhomogeneities,[15–20] but the results do not describe the entire behavior as we will show in this work. To understand the prospects and limitations of self-heating, a description of the OLED at strong self-heating is required.

Recently, it has been revealed that organic semiconductors do essentially show the behavior of thermistor devices.[21] A thermistor is an electronic device with a strong temperature dependence of the conductivity, often described by an Arrhenius law

$$\sigma(T) = \sigma_0 \exp(B/T) \quad (1)$$

where σ_0 is a reference conductivity, T is the temperature, and B is the temperature coefficient. In the case of organic semiconductors, $B < 0$ is a negative temperature coefficient (NTC), and thus the conductivity increases under rising temperature. If a constant voltage is applied, this can lead to a strong positive feedback loop between power dissipation and current flow, finally leading to a thermal runaway phenomenon in which an electronic device shows a switching from a rather low current density branch to a branch with a very high current density.[21,22] Normally, this induces the destruction of the device by thermal breakdown. It is known that a thermistor can be stabilized by using a resistor in series, and thus bistability is suppressed.[23] However, at relevant currents, the thermistor will still enter into a region of negative differential resistance (NDR) which is the mathematical reason for the switching phenomena. As a consequence, NTC-thermistors have an S-shaped current-voltage (IV) characteristic, in contrast to several other effects inducing N-shaped NDR (N-NDR), for example, by resonant tunneling or due to interface traps.[24,25] In OLEDs, as a representative for organic semiconductor devices, to the best of our knowledge such effects have not been demonstrated or they have just led to uncontrolled destruction of the devices.[26] One reason could be the fact that the transparent electrode introduces both a sheet resistance and an external series resistance, limiting the current and hiding an S-shaped behavior of the IV curve. Hence, the challenge consists in demonstrating the presence of an NDR effect induced by self-heating in OLEDs and to find out how the zero-dimensional thermistor model introduced in the literature[21] behaves in a spatial configuration where the lateral expansion of the active area is huge with respect to the thickness, so that the current has to flow through vertically. Due to the outcoupled light which is roughly proportional to the current flow, OLEDs would provide a perfect model system, allowing to study the effects in detail.

2. Results

2.1. Improved Setup: 4-Wire Crossbar Measurements

For measuring possible NDR effects due to self-heating, we have created a new measurement setup, called 4-wire crossbar. **Figure 1**d visualizes this setup in a topview of an OLED crossbar structure. In a usual current-voltage measurement, the two different electrodes are contacted from a single side to apply a low (*V*–) and a high (*V*+) potential. Between these potentials, the total current I flows, realized by a current source. However, since electrodes overlap the active area, a second contact can be connected to each electrode to sense the potential which is present at the opposite side. For each electrode, independently whether the potential is low (*S*–) or high (*S*+), a sensing contact can be applied. The voltage S between both sensing contacts

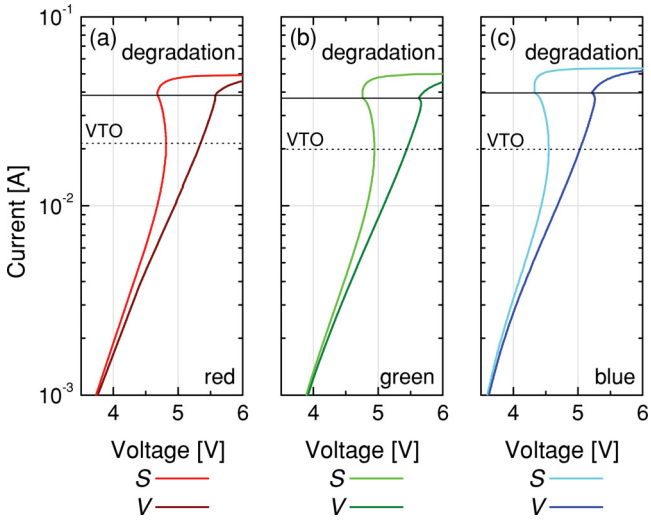

Figure 2. IV characteristics of the 4-wire crossbar measurement for a red, green, and blue OLED. The total current is plotted over the voltage *V*, to drive the current and the measured voltage *S* at the sensing contact. Starting with 20 mA voltages are decreasing with increasing current, indicating the NDR effect. A dotted line denotes this voltage turnover (VTO). This happens before samples degrade due to overheat in the range between 35 mA and 40 mA, corresponding to device temperatures around 60 °C (Supporting information, Figure S3).

can be measured and compared to the originally applied voltage *V* between *V*– and *V*+. The idea of this setup is that whenever a NDR will appear in the device, problems arising in two terminal measurements can be avoided, including the impact of the series resistance of the ITO outside the active area or the fact that thermal runaway occurs which eventually destroys the device. However, with additional sensing contacts, it might be possible to detect the voltage decrease inside the device, since it is a typical feature of 4-wire measurements that a series resistance is excluded.

For measurement, we use standardized samples which are used for tracking purposes to continuously check processing quality (Supporting Information, Figure S2). Similar OLED configurations have been published elsewhere.[27,28] To realize a 4-wire crossbar measurement, the encapsulation is removed in a glovebox while their current-voltage characteristics remain unchanged. A picture of a sample after measurement can be seen in Figure 1e. The measurements performed during operation of a red, green, and blue OLED are shown in Figure 1a–c.

The results are plotted in **Figure 2** for a current sweep from 1 mA until degradation appears, with 500 values per decade. First, we will concentrate onto the current plotted over the applied voltage *V*. The corresponding data coincide with a normal 2-wire measurement. With rising voltages the current also rises until ≈ 40 mA (solid black lines) are reached which will unavoidably lead to the degradation of the sample due to self-heating. Since these OLED layer structures become high-Ohmic while degrading, the applied voltage *V* rises caused by the constant current mode. Thus, the dissipated power increases and heats up the device, accelerating the degradation and starting with a kink in the IV curves. This point lies in a temperature range between 60 °C and 65 °C (Supporting Information, Figure S3). Besides this, a 2-wire measurement of an OLED will not disclose any special effects.

Now, we will focus on currents plotted over the sensed voltage *S*. In contrast to the previous measurement, a qualitatively different result is obtained. Beginning from 1 mA, both types of curve deviate from each other, revealing the beginning of self-heating. Most interestingly, by reaching about 20 mA, the sensed contacts show a voltage turnover, clearly distinguishable from the onset of the degradation. By thermal imaging of an encapsulated sample we estimate an upper limit of the maximum temperature in the range of 45 °C (Supporting Information, Figure S1). Furthermore, the stability and reversibility of the effect is checked by a well-defined forward and backward sweep (Supporting Information, Figure S4). As a result, the 4-wire crossbar measurement clearly proves the presence of an S-shaped NDR due to self-heating in a red, a green, and a blue OLED, similar to our observation in a previous work for C60 devices.[21] The capability to measure self-heating is further proven by the fact that a change of the thermal environment (Supporting Information, Figure S6) shifts the voltage turnover, whereas the currents and voltages around 1 mA remain similar. Additionally, we can exclude several other effects causing NDR in OLEDs as they exhibit an N-shaped IV curve.[25,29–33]

2.2. Electrothermal OLED Simulations

The voltage *V* and the voltage *S* differ under self-heating, and thus it is expected that the voltage within the device is not uniform anymore, leading to inhomogeneous current transport and heat dissipation. With the help of an electrothermal network simulation, we try to understand the processes taking place in the OLED. In another study,[21] a product ansatz of an isothermal power law current-voltage characteristic and an Arrhenius like conductivity-temperature law has been successfully used to explain S-NDR phenomena in n-doped/intrinsic/n-doped C60 devices given by

$$I(V,T) = I_{\mathrm{ref}}\left(V/V_{\mathrm{ref}}\right)^{\alpha}\exp\left[-E_{\mathrm{act}}/k_{\mathrm{B}}\left(1/T-1/T_{\mathrm{a}}\right)\right] \quad (2)$$

where α is the exponent of the power law, T is the temperature, E_{act} is the activation energy of the conductivity, and T_{a} is the ambient temperature. The implementation of this thermistor model for the multi-physics network simulation is based on a study published elsewhere.[34] Comparison with the analytic solution proves the correct function for one thermistor in series with a resistor (Supporting Information, Figure S7). An array of $(m = 10) \times (n = 10)$ thermistor devices now represents the active area and the current of each thermistor I_{ij} equals the charge flow through the OLED layer stack for a certain part of the active area. For simplicity, it is assumed that the metal electrode (cathode) of the OLED has such a low sheet resistance in comparison to the ITO (anode) that its influence can be neglected. Thus, all upper cathode contacts of the thermistor array are connected to each other. The anode is modeled by connecting all upper electrical contacts of the thermistor array via a network of resistors corresponding to a sheet resistance of 26.5 Ω. Furthermore, the thermistor array is coupled to a thermal network, modeling both the glass substrate and the heat transport

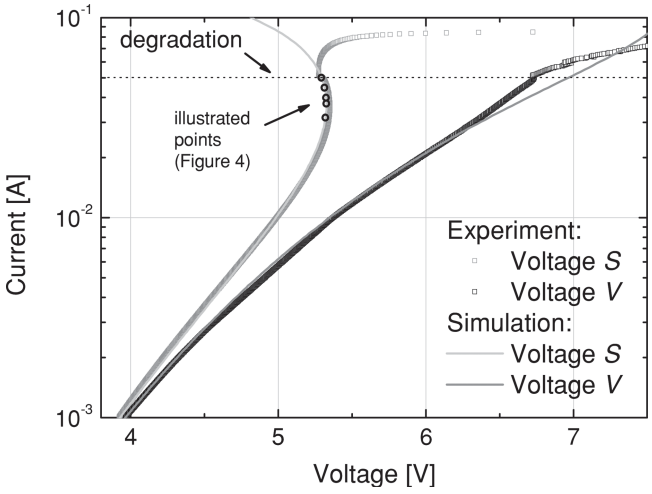

Figure 3. Simulated and measured IV characteristics of the 4-wire crossbar experiment on the green OLED. The simulation of the sensing voltage *S* reproduces the experiment up to the point where the device starts to degrade. Small black circles indicate the currents at which simulated current density and temperature are presented in Figure 4.

into the environment. In this thermal network, a resistor corresponds to a thermal resistance, a voltage represents a temperature difference, and a current represents a heat flow. The thermal network is a 3D resistor network and includes regions outside the electrically active area. Detailed network schemes and further informations can be found within the Supporting Information in Figures S11–S13. Besides heat generated by the thermistor devices, the simulation incorporates voltage drops along the anode, producing a further heat source fed into the thermal network.

For a comparison between experiment and simulation, further 4-wire crossbar measurements are performed on a green OLED, mounted onto a copper block. The results are shown in **Figure 3**.

The power law describing the isothermal current-voltage characteristic of the OLED is easily fitted by defining a reference point where no self-heating occurs. In our example, this is $I_{ref} = 1$ mA and $V_{ref} = 3.942$ V, so that the IV curve of the total thermistor array is fixed to this point, and the correct increase can be tuned by adjusting the exponent of the power law to $\alpha = 8.7$. The fact that a part of the applied power is coupled out as light is considered by reducing the generated heat by 20%. For simplicity, this value is kept constant.

The thermal system of the OLED can be described by a heat flow downwards into the glass substrate and upwards into the nitrogen atmosphere. A lateral flow to the substrate given by the thin electrodes or the organic molecular layers is neglected (see elsewhere).[35] The use of a simplified resistor network to model the heat transfer requires a well-defined and easy to describe thermal system. Therefore, we fix the glass substrate to a copper block via heat sink paste to ensure proper thermal contact. The heat transfer from the OLED into the glass substrate and from the glass substrate into the copper block is supposed as ideal. Since the large copper block has a high heat conductivity (400 W m^{-1} K^{-1}), its temperature can be assumed to correspond to the ambient temperature T_a. Thus, the limiting factor for heat transport is the thermal conductivity of glass, chosen to be 1.8 W m^{-1} K^{-1}. In the simulation, a variation of this parameter shifts the point of the voltage turnover to higher or lower currents along the normally measured curve. For the heat flow upwards from the OLED to air, we use a rather overestimated coefficient of 10 W m^{-2} K^{-1}, anyhow still realizing a minor heat flow with respect to that realized by the glass substrate and the copper block.

Besides modeling the thermal environment, the most important parameter of the system is the activation energy E_{act} of the OLED, used in Equation 2. This parameter influences the shape of the sensed current-voltage curve, leading to a stronger curvature with increasing activation energy (see in literature).[21] By using $E_{act} = 25\ k_B T_a$, a good agreement between experiment and simulation is achieved. Within the Supporting Information (Figure S3, Supporting Information), temperature dependent IV measurements reveal activation energies between 13 $k_B T_a$ and 34 $k_B T_a$ for different voltages at temperatures from −30 °C to 30 °C. At higher temperatures, extraction of suitable values is influenced by self-heating, but most disturbingly, series resistances of the electrodes and the setup will limit the current flow, decreasing the real voltage drop of the OLED. This results in underestimated activation energies. More details about implementation of the parameters can be found in the supporting information. Although this model of thermistors, electrical resistors, and thermal resistors is quite simple, it accounts for all qualitative aspects of the system described above, and furthermore it allows to reproduce the experimental results, as visualized in Figure 3. Degradation effects above 50 mA are not incorporated, and no agreement can be achieved above this value.

A closer look into the simulated distribution of currents and temperature is given in **Figure 4** for five different values of the total device currents as shown in Figure 3. Each picture shows the active area of the OLED sample. The electrodes are connected as visualized in Figure 1d, meaning that the current essentially flows from the left side (ITO) through the OLED stack and leaves at the bottom side via the metal electrode. With increase of the total current, the current density in the device will strongly rise in the left region of the active area while at the opposite side the current seems to change less. A similar behavior can be seen for the temperature increase which appears more widened but still is mainly located close to the left edge of the active area. Significant is that both current density and temperature rise tend to consolidate more and more towards the left region whereas close to the right edge they remain nearly unaffected by changes of the total applied current or voltage.

From the fact that declining voltages have been obtained in Figure 2, it is essential to investigate the local current I_{ij} and the local voltage V_{ij} in terms of NDR. Therefore, we define the local differential resistance

$$R_{diff,ij} = \frac{dV_{ij}}{dI_{ij}} \tag{3}$$

as the differential of the local voltages and currents across the OLED layers between top and bottom contact. To indicate the contour $R_{diff,ij} = 0$, a dark grey line is plotted in Figure 4, separating region I and region II. Region I behaves normally, having increasing currents while voltages are rising. In contrast, region II has a local NDR, and thus currents are rising

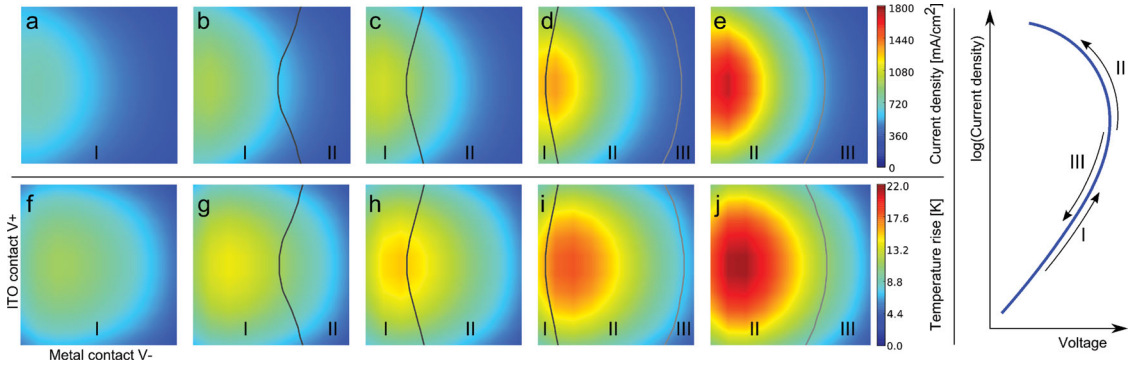

Figure 4. Simulated distributions of current density a–e) and temperature rise f–j) for total currents of 31.6 mA, 37.2 mA, 39.8 mA, 44.7 mA, and 50.1 mA as marked in Figure 3. The schematic diagram shows the three operation regimes in a current-voltage plot of a thermistor. Normal (I): Increasing current density and voltage. S-NDR (II): Increasing current density while voltage decreases. Switched-back (III): Both, current density and voltage decrease. The schematic IV curve visualizes the different operation modes for each thermistor.

under decreasing voltages. It is obvious that regions of NDR are shifting from the right to the left with the increase of the total device current. They appear first with the occurrence of the voltage turnover of the sensed voltage S in the 4-wire crossbar measurement.

However, by reaching a certain current level, a new region III enters into the device from the right. Surprising to us, this region has once more a positive differential resistance, similar to the normally behaving region I. To understand this phenomenon, the differential resistance has to be analyzed in more detail. In **Figure 5**, a table of four possible configurations is shown. For example, the local change in voltage is characterized by $\mathrm{d}V_{ij}/\mathrm{d}V$, and analogously for currents, $\mathrm{d}I_{ij}/\mathrm{d}I$ characterizes the local change in current. In a normal operation mode, currents and voltages increase at the same time with their external counterparts, while in an S-shaped NDR (S-NDR) region, local currents I_{ij} will increase for decreasing voltages V_{ij}. A very interesting configuration is realized when local currents and voltages decline at the same time even though externally applied currents and voltages increase further. By comparison of the individual terms within the simulation result, it is found that in region III the OLED indeed shows such a strange behavior. It can be fully understood if one reminds the decreasing local voltages in region II. Due to the fact that the ITO electrode is contacted from the left side, OLED regions at the opposite side might not generate enough power dissipation to heat up and reach a NDR. Then

current \ voltage	$\frac{dV_{ij}}{dV} > 0$	$\frac{dV_{ij}}{dV} < 0$
$\frac{dI_{ij}}{dI} > 0$	$\frac{dV_{ij}}{dI_{ij}} > 0$ normal (I)	$\frac{dV_{ij}}{dI_{ij}} < 0$ S-NDR (II)
$\frac{dI_{ij}}{dI} < 0$	$\frac{dV_{ij}}{dI_{ij}} < 0$ N-NDR (not present)	$\frac{dV_{ij}}{dI_{ij}} > 0$ switched-back (III)

Figure 5. The table visualizes the four different types of differential resistance. In a thermistor array, three of them are possible: normal (I), S-NDR (II), and switched-back (III).

they are supplied with the reduced voltage after the lateral passage of the NDR region (II). Since this region has declining voltages, in region III the OLED layer stack does only "notice" a declining voltage and consequently the current density is switched back. To give a simpler picture of that mechanisms, we provide calculations of three parallel thermistors coupled by series resistors, compare Figure S8 and S9 of the supporting information. There it is shown that in a one-dimensional thermistor chain, all thermistors behind the first one are instantly switched back if no thermal coupling exists between them. If thermal coupling is incorporated, due to the heat exchange between individual thermistors, the abrupt switch back is replaced by a smoother transition similar to the simulations of the two dimensional thermistor array presented in Figure 4.

The fourth configuration in Figure 5 is a decrease of the current accompanied by increasing voltages. This operation mode would correspond to an N-shaped NDR and is not present in this system due to the nature of the self-heating phenomena. The operation of region I, II, and III is further visualized in the schematic IV curve of Figure 4. Please note, however, that due to the thermal coupling, every thermistor in the network has its own dependence $I(V,T)$ on voltage and temperature.

2.3. Large Active Area Lighting Panel

Previous crossbar measurements show that the distribution of current becomes strongly inhomogeneous when the NDR effect arises. It remains an open question whether these effects also impact onto OLED applications like lighting.

For that reason, we investigate the luminance distribution of an opaque Tabola lighting panel (produced by Fraunhofer COMEDD, Dresden) with an active area of 15 cm × 7.5 cm. This tile size is representative for present-day OLED lighting applications. The metallic electrode has its contacts to the power supply at the four corners and the ITO electrode is contacted via a metallic frame all around the active area. Please find more details on the Tabola within the supporting information. The centered cross-section of the luminance for the longer device width is shown in **Figure 6**a. While these lighting

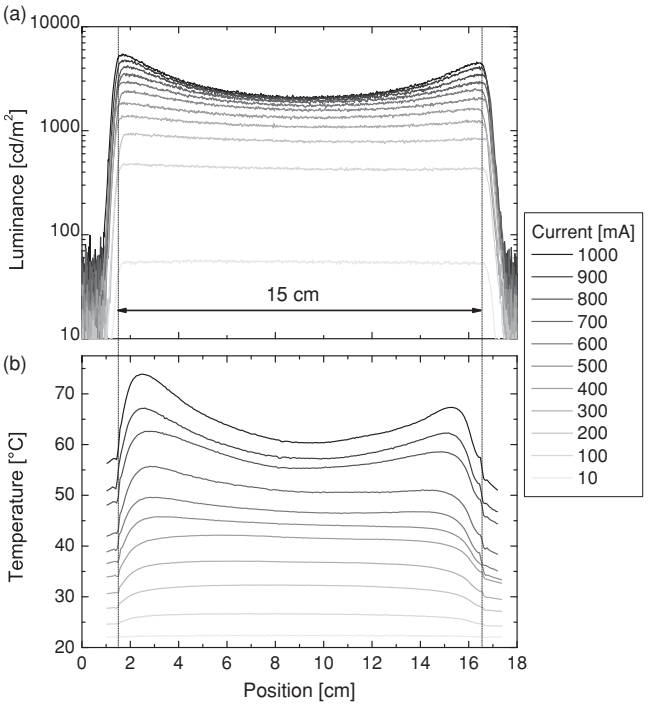

Figure 6. Measured a) luminance and b) temperature profiles of a warm white lighting panel with the dimensions 15 cm × 7.5 cm. At 1000 cd m^{-2}, the homogeneity is alright, but it drastically changes under self-heating. Starting around 500 mA the luminance in the center of the device saturates and hardly exceeds 2000 cd m^{-2}, whereas the luminance in the maximum region still linearly increases (Supporting Information). We exclude a degradation at the center of the lighting panel, since highest temperatures should rather effect the outer regions. Consequently, the reduction of luminance is related to the formation of a switched-back region which further implies already the existence of NDR regions in the device at lower currents.

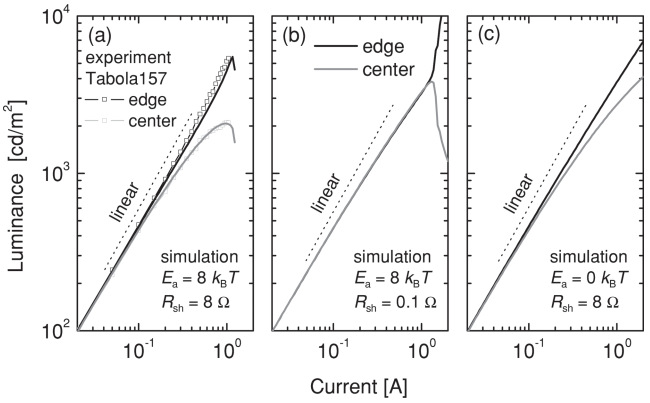

Figure 7. Comparison between experiment and simulation for the luminance at the center and the midpoint of the shorter edge. a) Measured luminance at the edge and at the center of the lighting panel vs. simulation results. Up to a current of 1 A, a strong effect of sample degradation can be excluded. b) Simulation with reduced sheet resistance. c) Simulation with no activation energy.

panels have a high brightness homogeneity around 1000 cd m^{-2} (≈200–300 mA), and are still acceptable for 2000 cd m^{-2}, with increasing current, luminance will only increase at the edges, but the center position shows a saturation of luminance. One might expect the central region to be hottest and thus degradation processes will take place there, but this is not the case as revealed in Figure 6b. At the highest currents, the temperature distribution shows two maxima which are located close to the edges. This might seem surprising, since the center of the lighting panel is supposed to face the worst conditions to conduct away the heat. However, the power dissipation close to the edges strongly rises with respect to the central region. In **Figure 7**a, experimental values of the luminance vs. total device current are presented for a position at the edge and at the center for the cross-section, shown in Figure 6a. It becomes obvious that both curves begin to split shortly before 2000 cd m^{-2} are reached. In this double logarithmic plot the luminance at the center does hardly increase anymore while the luminance at the edge position seem to increase even slightly super linearly. If we consider the typical efficiency roll-off [36–39] of an OLED at high current densities, a weaker increase of luminance over current is expected.

To clarify this, we adopt the network model, described above, onto the geometry of the Tabola lighting panel. Please find further details within the supporting information. The fully metallic electrode is assumed to have a negligible sheet resistance and for the bottom ITO electrode, responsible for light outcoupling through the substrate, a sheet resistance of 8 Ω is used as measured with a common 4-point probe setup. Again, the isothermal current-voltage characteristic of the device is fitted by a power law applied to a point (I_{ref} = 10 mA, V_{ref} = 7.2 V) where no self-heating appears and high current homogeneity can be assumed. To account for the current efficiency roll-off, we fit this value over various currents where a homogeneous brightness is given (Supporting Information, Figure S16). With the help of the analytical expression, luminance values are calculated from the simulated current density. However, for the reason of simplicity, the generated heat is still reduced by a constant value of 20% due to light outcoupling. The most important parameter of the simulation is the activation energy chosen to be 8 $k_B T_a$. This value, significantly below the activation energies necessary to simulate the small active area OLEDs in the section above, can be justified by the fact that the white light of the Tabola lighting panel is created by multiple color OLED layer stacks connected in series.

Under these reasonable assumptions, the experimental values in Figure 7a are reproduced over the measured current range. For comparison, a simulation with a small sheet resistance of the ITO electrode and with no activation energy assumed are shown in Figure 7b,c, respectively. In both cases, the simulation behaves quite differently.

The saturation of brightness in the center can be understood by the visualization of the simulated luminance and the occurrence of the normal region (I), the NDR region (II), and the switched-back region (III) in **Figure 8**. Due to the rectangular geometry and the anode contacted from all sides, first NDR regions appear around 0.85 A inside the active area at two different locations. After they have merged, this region is growing towards the edges. At around 1 A, a switched-back region appears first in the center of the lighting panel

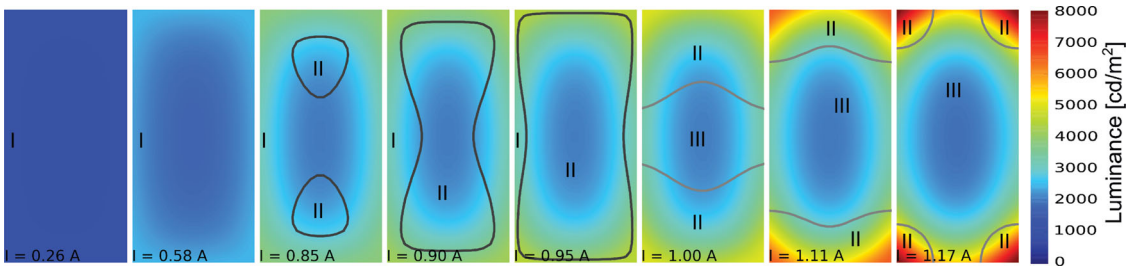

Figure 8. Each picture corresponds to a simulated luminance distribution of a 15 cm × 7.5 cm large Tabola lighting panel. At 0.26 A, the luminance of around 1000 cd m^{-2} is very homogenous, changing when the current is increased twice. Around 0.85 A, first regions with local NDR (II) appear. Around 1 A, all normal regions (I) have vanished and the first switched-back region (III) appears. Dark grey lines separate regions I and II whereas bright grey lines separate regions II and III.

and expands subsequently to the nearest edges. This is the reason why the simulation predicts a saturation accompanied by a return of the luminance in the central region. With that knowledge we estimate that the central region of the Tabola lighting panel has reached or is shortly before entering the switched-back operation mode at the highest measured currents, and it is likely that larger parts of the device already show local NDR. However, with the further expansion of the switched-back region, the current distribution of the device will become unstable due to the fact that any additional rise of the total current will lead to an extreme current increase in the residual NDR regions, located at the corners, enhanced by the current reduction in the switched-back regions. This explains why the luminance at the edges increases linearly or slightly stronger with current, even though current efficiency roll-off takes place.

We would like to mention that the simulation reveals a switching phenomenon into a more stable electrothermal configuration (not shown) when the total current exceeds 1.24 A (Figure 7a). It will be the topic of further investigations to study these aspects in more detail.

3. Conclusion

We demonstrate that irrespective of the device area, OLEDs show such a strong electrothermal feedback that S-shaped negative differential resistance will occur, as predicted by the self-heating theory assuming an Arrhenius like conductivity-temperature law. By using 4-wire crossbar measurements, this has been clearly proven by experiment for a red, green, and blue OLED. This technique is ideal to investigate the influence of several parameters like activation energy of the OLED, sheet resistance of the electrodes, or simply the series resistance of the setup. Further multi-physics network simulations demonstrate that an OLED can essentially be understood as a two dimensional array of temperature activated thermistor devices. Upon self-heating, regions with local NDR appear. As a further consequence, these regions are able to switch back regions located at a larger distance from the contacts. Thus, central regions or regions far away from the edges show a saturation or even a decrease in current, even though the total current and voltage applied to the device are still increasing. This explains the dramatic increase of brightness inhomogeneities in a white OLED lighting panel when self-heating occurs in a pronounced manner. Our results are able to explain the most fundamental processes taking place in OLED devices under self-heating and can be adapted to similar thin film devices. In the future, simulations based on temperature-activated charge transport are expected to provide a deeper insight into the limitations of OLED lighting panels and applications. It will be of interest to investigate the origin of the activation energy by the different functional layers of the OLED. If it can be decreased, device function at elevated currents could guarantee higher brightness combined with untainted appearance of the OLED tiles and reducing the risk of electrothermal instabilities or switching phenomena.

4. Experimental Section

OLEDs for 4-wire crossbar measurements are fabricated by thermal vapor deposition in high vacuum. After cleaning of the prestructured ITO glass substrates, a p-doped/intrinsic/n-doped layer configuration is realized, using 30 nm MeO-TPD:F6TCNNQ (2 wt%), 10 nm NPB, a 20 nm thick emitter system, 10 nm BAlq2, 30 nm BPhen:Cs (ratio: 1:1). F6TCNNQ is purchased from Novaled AG (Dresden, Germany). 100 nm Al realize the top electrode. For the emitter system, 20 nm MADN:TBPe (1.5 wt%) (blue), 6 nm TCTA:Ir(ppy)3 (8 wt%) and 12 nm TPBI:Ir(ppy)3 (8 wt%) (green), 20 nm NPB:Ir(MDQ)2(acac) (10 wt%) (red) are used. The glass substrate has a size of 2.54 cm in square and a thickness of 1.1 mm. The active area is approximately $(2.54\ mm)^2$. 4-wire crossbar measurements are carried out with two source-measuring units Keithley 2400 controlled by a home built software. Network simulations are made by the freely available program LTSpice IV (Linear Technology) and a self-made circuit generator script. Results are evaluated with a self-made program using matplotlib for plotting the data. The simulation results are interpolated (contourf-function, linear interpolation) which does not change the value range or the local occurrence of NDR regions. Temperature and luminance measurements are done by an IR camera VarioTHERM head II (company: JENOPTIK AG) calibrated with a thermo sensor PT1000 and a video photometer PR-905 from PhotoResearch Inc. The opaque Tabola lighting panel is fabricated at Fraunhofer COMEDD (Dresden, Germany) and uses a 3-unit-stacked architecture based on a fluorescent blue, phosphorescent green and phosphorescent orange unit.

Supporting Information

Supporting Information is available from the Wiley Online Library or from the author.

Acknowledgements

The authors thank Simone Hofmann and Caroline Murawski for discussions and help with the measurement setup. This work was financed by the European Community's Seventh Framework Programme under Grant Agreement No. FP7–267995 (NUDEV) (A.F.). Support from the excellence cluster cfaed is gratefully acknowledged. This work received funding from the Deutsche Forschungsgemeinschaft (DFG) within the DFG Research Center MATHEON under project D22 (A.G.) and the DFG CRC 787 "Semiconductor Nanophotonics" (T.K.) Part of this work was funded with support from the Free State of Saxony and the European Commission (EFRE) within the project Next-O-Light (100135204) (J.B.).

Received: September 2, 2013
Revised: November 28, 2013
Published online: February 4, 2014

[1] K. T. Kamtekar, A. P. Monkman, M. R. Bryce, *Adv. Mater.* **2010**, *22*, 572–582.
[2] B. Geffroy, P. le Roy, C. Prat, *Polym. Int.* **2006**, *55*, 572–582.
[3] Y.-S. Tyan, *J. Photonics Energy* **2011**, *1*, 011009–011009.
[4] S. Reineke, F. Lindner, G. Schwartz, N. Seidler, K. Walzer, B. Lüssem, K. Leo, *Nature* **2009**, *459*, 234–238.
[5] Press release LGChem 2013/04/10. http://www.lgchem.com/lgchemoled/LGOLED_04_01_01.jsp?PR_NO = 6 (accessed: September 2013).
[6] K. Neyts, M. Marescaux, A. U. Nieto, A. Elschner, W. Lovenich, K. Fehse, Q. Huang, K. Walzer, K. Leo, *J. Appl. Phys.* **2006**, *100*, 114513–4.
[7] J. Park, J. Lee, Y.-Y. Noh, *Org. Electron.* **2012**, *13*, 184–194.
[8] M. Slawinski, M. Weingarten, M. Heuken, A. Vescan, H. Kalisch, *Org. Electron.* **2013**, *14*, 2387–2391.
[9] Y.-S. Tsai, S.-H. Wang, C.-H. Chen, C.-L. Cheng, T.-C. Liao, *Appl. Phys. Lett.* **2009**, *95*, 233306–3.
[10] S. Chung, J.-H. Lee, J. Jeong, J.-J. Kim, Y. Hong, *Appl. Phys. Lett.* **2009**, *94*, 253302–3.
[11] J. Park, H. Ham, C. Park, *Org. Electron.* **2011**, *12*, 227–233.
[12] L. Yang, B. Wei, J. Zhang, *Semicond. Sci. Technol.* **2012**, *27*, 105011.
[13] A. A. Zakhidov, S. Reineke, B. Lüssem, K. Leo, *Org. Electron.* **2012**, *13*, 356–360.
[14] H. Sasabe, J. Kido, *Chem. Mater., Chem. Mater.* **2010**, *23*, 621–630.
[15] C. Gärditz, A. Winnacker, F. Schindler, R. Paetzold, *Appl. Phys. Lett.* **2007**, *90*, 103506–3.
[16] A. W. J. Gielen, M. Barink, J. van den Brand, A. M. B. Van Mol, *10th International Conference on Thermal, Mechanical and Multi-Physics Simulation and Experiments in Microelectronics and Microsystems, EuroSimE 2009*, IEEE W, 1–6.
[17] X. Qi, S. R. Forrest, *J. Appl. Phys.* **2011**, *110*, 124516–11.
[18] M. Slawinski, D. Bertram, M. Heuken, H. Kalisch, A. Vescan, *Org. Electron.* **2011**, *12*, 1399–1405.
[19] L. Pohl, E. Kollár, A. Poppe, Z. Kohári, *Microelectron. J.* **2012**, *43*, 624–632.
[20] P. Schwamb, T. C. Reusch, C. J. Brabec, *Org. Electron.* **2013**, *14*, 1939–1945.
[21] A. Fischer, P. Pahner, B. Lüssem, K. Leo, R. Scholz, T. Koprucki, K. Gärtner, A. Glitzky, *Phys. Rev. Lett.* **2013**, *110*, 126601.
[22] (Eds: M. Shaw , N. Yildirim, P. W. Hawkes) , The Physics of Instabilities in Solid State Electron Devices *60* Academic Press, New York **1983**, 307–385.
[23] E Schöll, Nonequilibrium Phase Transitions in SemiconductorsSpringer Berlin Heidelberg **1987**.
[24] L. Esaki, L. L. Chang, *Phys. Rev. Lett* **1974**, *33*, 495–498.
[25] J. Chen, L. Xu, J. Lin, Y. Geng, L. Wang, D. Ma, *Appl. Phys. Lett.* **2006**, *89*, 083514.
[26] L. Pohl, E. Kollar, *17th International Workshop on Thermal Investigations of ICs and Systems (THERMINIC), IEEE* **2011**, 1–6.
[27] R. Meerheim, R. Nitsche, K. Leo, *Appl. Phys. Lett.,* **2008**, *93*, 043310–3.
[28] C. Weichsel, S. Reineke, M. Furno, B. Lüssem, K. Leo, *J. Appl. Phys.* **2012**, *111*, 033102–7.
[29] V. Cimrova, D. Neher, *Synth. Met.* **1996**, *76*, 125–128.
[30] S. Berleb, W. Brütting, M. Schwoerer, *Synth. Met.* **1999**, *102*, 1034–1037.
[31] S. Y. Ryu, S. J. Jo, C. S. Kim, S. H. Choi, J. H. Noh, H. K. Baik, H. S. Jeong, D. W. Han, S. Y. Song, K. S. Lee, *Appl. Phys. Lett.* **2007**, *91*, 093515.
[32] Y.-K. Fang, Y.-T. Chiang, S.-F. Chen, C.-Y. Lin, S.-C. Hou, C.-S. Hung, T.-Y. Tsai, S.-H. Chang, T.-H. Chou, *J. Phys. Chem. Solids* **2008**, *69*, 738–741.
[33] J. Lin, D. Ma, *J. Appl. Phys.* **2008**, *103*, 124505.
[34] A. Ü. Keskin, *Sens. Actuators A: Phys.* **2005**, *118*, 244–247.
[35] A. Fischer, P. Pahner, B. Lüssem, K. Leo, R. Scholz, T. Koprucki, J. Fuhrmann, K. Gärtner, A. Glitzky, *Org. Electron.* **2012**, *13*, 2461–2468.
[36] G. Schwartz, S. Reineke, K. Walzer, K. Leo, *Appl. Phys. Lett.* **2008**, *92*, 053311–3.
[37] N. C. Giebink, S. R. Forrest, *Phys. Rev. B* **2008**, *77*, 235215.
[38] S.-J. Su, E. Gonmori, H. Sasabe, J. Kido, *Adv. Mater.* **2008**, *20*, 4189–4194.
[39] C. Murawski, K. Leo, M. C. Gather, *Adv. Mater.* **2013**, *25* 47 6801–27.